

Article

A Study of the Effects of Time Aggregation and Overlapping within the Framework of IEC Standards for the Measurement of Harmonics and Interharmonics

Angel Arranz-Gimon ¹, Angel Zorita-Lamadrid ², Daniel Morinigo-Sotelo ²  and Oscar Duque-Perez ^{2,*} 

¹ Department of Electronic Technology, Universidad de Valladolid, 47011 Valladolid, Spain; gimon@tele.uva.es

² Department of Electrical Engineering, Research group ADIRE, ITAP, Universidad de Valladolid, 47011 Valladolid, Spain; zorita@eii.uva.es (A.Z.-L.); daniel.morinigo@eii.uva.es (D.M.-S.)

* Correspondence: oscar.duque@eii.uva.es; Tel.: +34 983184533

Received: 23 September 2019; Accepted: 24 October 2019; Published: 26 October 2019



Abstract: The increasing incorporation of power electronics and other non-linear loads, in addition to their energy advantages, also implies a poor power quality, especially as regards harmonic pollution. Different solutions have been proposed to measure harmonic content, taking the International Electrotechnical Commission (IEC) standards as a reference. However, there are still some issues related to the measurement of the harmonic, and especially, interharmonic content. Some of those questions are addressed in this work, such as the problem derived from the instability of the values obtained by applying the discrete Fourier transform to each sampling window, or the appearance of local peaks when there are tones separated by multiples of the resolution. Solutions were proposed based on time aggregation and the overlapping of windows. The results demonstrate that aggregation time, window type, and overlapping can improve the accuracy in harmonic measurement using Fourier transform-based methods, as defined in the standards. The paper shows the need to consider spectral and time groupings together, improving results by using an appropriate percentage of overlap and an adaptation of the aggregation time to the harmonic content.

Keywords: Harmonic analysis; interharmonics; spectral leakage; rectangular window; Hann window; time aggregation; overlapping; power quality

1. Introduction

Power quality is an essential feature in modern electrical systems. The increase in the number of time-variant and non-linear loads and the proliferation of distributed generation is affecting the performance of electric networks [1,2]. One of the main aspects to take care of is the harmonic content. Nonlinear loads and switched devices produce harmonics and interharmonics, increasing energy losses and producing measurement errors, equipment overheating, communication interferences, and light flicker [3,4]. New technologies, such as smart metering, renewable energy sources, electric vehicles, and other end-user equipment connected to the grid through static converters are responsible for interharmonic emissions in the range above 2 kHz (known as supraharmonics); thus, expanding the interest of researchers on energy quality [5,6].

With the increase of non-linear loads in power systems, interharmonics are becoming a growing concern [7,8]. The presence of interharmonics complicates the analysis and measurement due to the change of the periodicity of the waveform and a greater sensitivity to desynchronization problems. All this leads to the appearance of spectral leakage when applying methods based on the Fourier

transform, giving rise to instability and unreliability in the RMS (Root Mean Squared) values obtained by interacting with the leakage produced by nearby interharmonics.

In recent years, several signal processing methods have been proposed to enhance the identification of the interharmonic content [9–12]. Fourier transform, wavelet transform, Hilbert–Huang transform, and Chirp z-transform are the main non-parametric methods applied to power system waveform analysis. Parametric methods have been proposed too to perform the analysis, such as Kalman filters, ESPRIT (estimation of signal parameters by rotational invariance technique), MUSIC (multiple signal classification), and the Prony method. Hybrid methods provide high-frequency resolution and better estimation accuracy. Other modern techniques, such as enhanced the phase locked loop (EPLL), artificial neural network, and adaptive linear neural network (ADALINE) have also been used in power quality analysis. Parametric methods achieve higher frequency resolution, with tracking capabilities for time-varying harmonics and interharmonics, and are more suitable for interharmonic measurement than non-parametric methods. However, according to [11], these algorithms are time-consuming and not robust to noise and outliers, and their performance depends on the prior information of the order of the model. Non-parametric methods estimate harmonics directly from the signal, being less computationally expensive and easier to apply than parametric or hybrid methods [12]. The most common non-parametric method is the discrete Fourier transform (DFT), which is sufficiently robust and time-efficient, which justifies the use of DFT-based methods in power quality analyzers. However, the signal sampling time limits the frequency resolution and it may suffer from spectral leakage caused by fundamental frequency deviation and interharmonics [11].

The International Electrotechnical Commission (IEC) standards 61000-4-7 [13] and 61000-4-30 [14], propose the use of the DFT transform and describe the spectral and time groupings required to perform power quality measurements. Harmonic and interharmonic grouping simplifies the need to know the frequency location and amplitude of a single component. With frequency grouping, the 61000-4-7 standard aims to collect most of the spectral leakage produced within each group, minimizing the error due to this leakage that spreads out of the group, (although it also picks up more spectral leakage from outside of the group). Time grouping, contemplated in standard 61000-4-30, partially solves the information loss due to leakage, increasing the accuracy, especially in the total power, and thus minimizing the error due to the lack of stationarity of the signal. Besides, time aggregation also compresses the information [15] and reduces the effects of noise present in the signal.

These standards are based on the application of the DFT transform with a rectangular window (RW) and a resolution or basic frequency of 5 Hz, for obtaining the RMS values of the harmonic and interharmonic groupings. The spectral leakage generated by the interharmonic tones (and, in general, by the tones not synchronized with the basic frequency) is its primary disadvantage. The main means to reduce this leakage are the correct synchronization of the acquisition windows to the fundamental, and the use of Hann windows (HW) only in the case of loss of synchronism. The performance of RW versus HW to minimize the effect of leakage is discussed in [15–20], where the results are compared to each of the frequency groupings defined in standard 61000-4-7. However, they do not present the development of the complete standard, taking into account the time grouping also described in standard 61000-4-30 and considering spectral and time groupings altogether, as it is done in this article.

Many other authors studied and use methods based on IEC standards. In [21–23], various DFT calculation methods are compared in the framework of IEC standards. In other articles, the IEC standard is used as a single method of measuring frequencies above 2 kHz [6,24,25] or as a reference technique to compare with other new high-frequency measurement methods [26–29]. Additionally, based on the IEC standards, in [30], the harmonic and interharmonic subgroups generated at the input of variable speed drives are analyzed; a fixed window width (tw) of 0.2 s and a fixed total aggregation time (Tw) of 3 s are used. Oliveira, Anesio, et al. study in [31] a methodology to identify the most appropriate sampling window to quantify harmonic and interharmonic emissions, considering variable signals in time, based on the calculation of harmonic and interharmonic distortions using the DFT according to IEC 61000-4-7. Bartman and Kwiatkowski in [32] compare the results obtained

with different total aggregation times, testing from windows of 0.2 s without time grouping to a total aggregation time of 3 s, as indicated in standard 61000-4-30.

Despite the works previously mentioned, the selection of an adequate aggregation time is still a challenge, as it is necessary to determine an appropriate value for the total aggregation time, which, according to the harmonic content of the analyzed signal, stabilizes and improves the accuracy of the results obtained with the DFT along the successive analysis windows. This is one of the main contributions of this paper: to demonstrate the improvement that involves an adequate time aggregation obtaining more reliable and accurate measures in all the RMS values calculated with the DFT for each spectral bar. This improvement can be extended to all the harmonic groupings and distortion rates defined in the standard and formed by those spectral bars [6,25,29,33], and to the distortion rates proposed by other authors and based on the same standard [6,33–37].

The signal processing recommended in the standards is aimed at standardizing, simplifying, and unifying the way of measuring signals from the supply network [21]. Nevertheless, there are many practical situations where the harmonic content differs significantly from the one in the supply network. A widespread example is a measurement in the output of frequency converters for controlling electric motors, whose harmonic contents differ in the low, and mainly, in the high-frequency range due to the modulation techniques used in the equipment [30,38,39]. These motor power signals present rich harmonic content, with multiple interharmonic tones, and in many cases, with amplitudes similar to those of their closest harmonics. These near-tone situations, whose leakage may interact, occur especially in frequency converters that use modulations, such as closed-loop [40] or random-type [41,42], or when connected to faulty motors which cause additional harmonic content [43–45].

This paper analyzes a problem caused by spectral leakage when IEC-based groups are obtained, especially when these are obtained from measurements on signals such as the output of electronic converters. The variability and unreliability of the RMS values obtained with the DFT in the successive sampling windows is the problem. This problem is caused by the interaction of the leakage produced by nearby tones when some of them are interharmonic tones not synchronized with the sampling window and of relatively large magnitude. It will be demonstrated how the time grouping and the choice of appropriate aggregation times specific to the type of signals measured at the output of inverters, and therefore adapting well those proposed in the regulations—will make it possible to reduce the effect of these variations due to leakage.

A second problem, related to the previous one, is the appearance of singularities or local peaks, due to interharmonic tones separated from each other by multiples of the spectral resolution and not affected by time aggregation as a way of obtaining a reliable RMS value. To correct this problem, this study developed a solution by aggregating with overlapping windows, that being the second main contribution of this paper.

The method proposed in this article improves harmonic and interharmonic identification using DFT-based methods, such as those defined in IEC standards, reducing spectral leakage effects by selecting a proper aggregation time. The proposed method also eliminates local peaks that appear in sensitivity curves by using overlapping windows. The proposed method was validated using synthetic signals and real signals coming from an induction motor, showing the advantages of this method over the one window DFT. Results demonstrate that, through the selection of an adequate aggregation time with an appropriate percentage of overlap, a response closer to the ideal can be achieved in all the frequency groupings defined in the standards; thus, more reliable and accurate measurements can be obtained in their related distortion rates.

The rest of this paper is organized as follows: Section 2 presents the problems of calculating amplitudes with DFT; these problems are caused by the interaction between several nearby tones, where at least one is not synchronized with the sampling window. First, a concrete case is examined, based on one of the examples described in the annex of standard 61000-4-7. General cases with any positions of frequencies are considered later, using the rectangular window. Next, in Section 3, a solution that minimizes these problems is studied using a simple and easy-to-implement technique,

such as time aggregation. This study is expanded in Section 4 by comparing the use of rectangular and Hann windows when several nearby tones interact. Then, in Section 5, particular cases not solved by time aggregation are studied, such as local peaks due to interharmonic tones separated by multiples of the frequency resolution. A solution to this new problem is developed based on time aggregation with overlapping between successive analyzed windows. Section 6 presents and analyzes experimental results, testing an induction, motor-fed with inverters with different harmonic contents, verifying that the aggregation time needed to stabilize the measurements depends on the harmonic content. Finally, the discussion and conclusions reached in this study are addressed in Section 7.

2. The Effects on Amplitude Due to Interactions between Tones

In this section, the problems derived when the DFT is performed following the indications of the IEC standard and when there is an interaction of the spectral leakage generated by nearby tones—are studied. First, a specific case based on an example proposed in the standard with several tones in fixed positions is analyzed. Next, some cases are studied with the rectangular window where the position between the different tones that interact is changed.

2.1. Analysis of the Effects of the Interaction between Tones

Spectral leakage is produced by interharmonic components of the signal or by desynchronization of the fundamental frequency (and all their integer multiples) to the sample window. To avoid spectral leakage when applying DFT, the sampling window must contain an integer multiple of all the periods of the frequency components of the signal. Optimally, this window is calculated as the minimum common multiple of all the contained periods and the resolution specified by IEC standards (5 Hz). The interharmonics can be due to the desynchronization of the fundamental with the sampling tw window (and consequently of all its multiples or harmonics), or due to actual interharmonic components, such as those generated by variable and non-linear loads, such as frequency converters.

If the existing harmonics and interharmonics in the signal are all multiples of the spectral resolution (of 5 Hz, for example), or if only one tone is taken into account, the possible time aggregation benefits are not appreciated, since the same absolute values are obtained with the DFT applied to every window, as in the cases analyzed in [16,17,19,20]. However, it will then be proven that the absolute value of the total vector changes if successive sampling windows of a signal with several nearby tones are analyzed. The spectral leakage of these tones may interact, as it is the case in signals composed by a harmonic tone and an interharmonic tone generating leakage. This variability is explained by the addition of the leakage vector to the fixed harmonic tone vector. The leakage vector rotates because its offset at the beginning of each window change.

An example was proposed, based on one described in the standard IEC 61000-4-7, Appendix C.4, to analyze the interaction between harmonic tones and the leakage produced by nearby interharmonics, and their relationship with time aggregation. A voltage waveform (Figure 1) with a 5th harmonic of 13.2 V, a 6th one of 10 V, and an interharmonic of 9.8 V at 253.3 Hz is considered. This interharmonic was added to the example of the standard since it is close to the 5th harmonic and far from the 6th one. This way, the effects of the relative situation between the leakage receiver harmonics and the interharmonics producing the leakage could be better observed.

Figure 1 shows the waveform of the signal in the time domain and the spectrum obtained using the DFT with a 0.6 s rectangular window. As the window used contained complete periods of all the components of the signal, no spectral leakage was observed. This ideal window was selected considering that the minimum common multiple of 250, 253.3, 300, and 5 Hz is 1.6 Hz. This ideal period (Tw) was also chosen as a multiple of $1/5$ Hz = 0.2 s so it could be synchronized with the window size proposed in the standard.

However, the harmonic composition of a signal is usually unknown, and following IEC standards, it was analyzed in successive short windows of 0.2 s, with leakage generally appearing in each of them. Therefore, total vectors with varying amplitudes in each successive short window analyzed were

obtained, due to the combination of representative vectors, which rotate at different speeds. The reason for choosing this short window size was the non-stationary nature of the signals analyzed and the time-resolution improvement at the cost of worsening the frequency resolution (uncertainty principle).

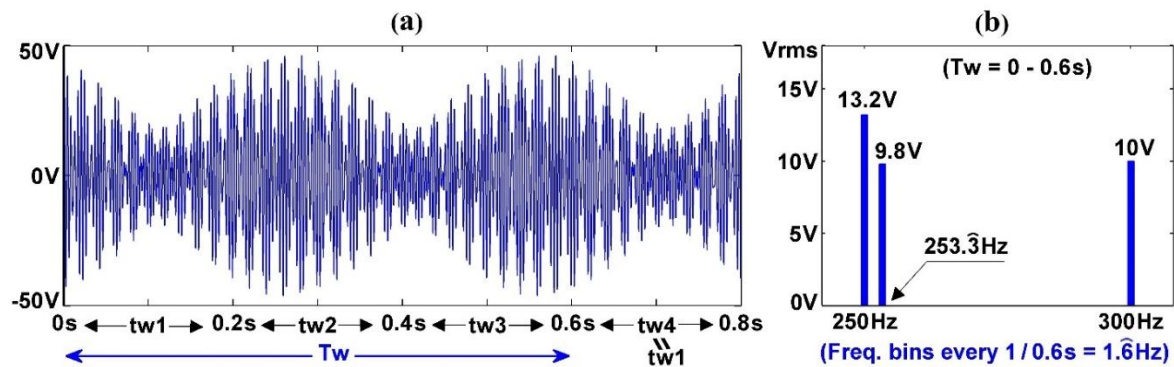


Figure 1. Example with signal composed by 5th and 6th harmonics and an interharmonic at 253.3 Hz: (a) waveform in the time domain, and (b) spectrum after using the discrete Fourier transform (DFT) in a single window of total aggregation time (T_w) = 0.6 s.

These changes of amplitude are illustrated in Figure 2a with the spectra for the first three short windows of the example of Figure 1. It can be observed how the total amplitude measured at the 250 Hz spectral bar changed since in that position the 5th harmonic and the leakage received from the close interharmonic at 253.3 Hz were added. The resulting vector oscillated between the sum of the modules or their difference, depending on the phase angle between the leakage vectors and the harmonic. The cycle was repeated every three windows, as can be expected since the ideal period in this example ($T_w = 0.6$ s.) is three short windows. In Figure 2, minor amplitude changes in the position of the farthest 6th harmonic can be seen. These changes are much smaller in the rest of the spectral bars, which only contain the received leakage (as can be seen in the resulting value of the interharmonic group gIH5).

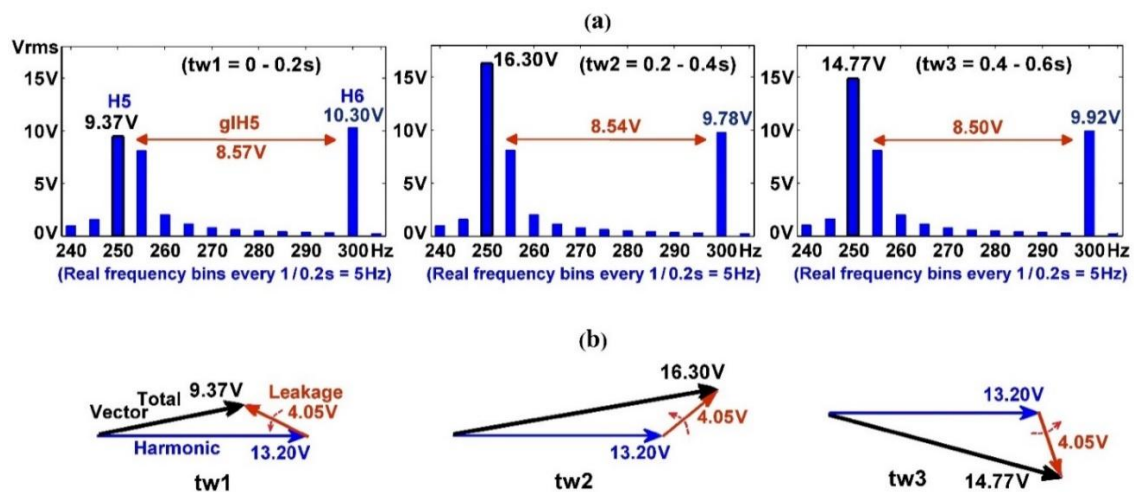


Figure 2. DFT on successive windows of 0.2 s of the signal of the example of Figure 1: (a) modules obtained, and (b) vector evolution of the 5th harmonic and its sum with the leakage received in the spectral bar of 250 Hz.

Therefore, the most important variations occur in the spectral bars corresponding to the harmonics closest to the interharmonics that generate spectral leakage when the DFT is applied to successive time windows. In these spectral bars, the leakage is projected on the fixed vector of the harmonic. The

spectral leakage phase is variable, so the resulting vector at the frequency of the harmonic can change considerably between successive collected windows, as illustrated in Figure 2b. It should be noted that the amplitudes of vectors represent the RMS values of the different measured frequency components.

Since leakage reduction is not always possible, at least the RMS value found measuring the harmonic content of each spectral bar must be stable and as close as possible to the RMS value of all the components added in that bar (or common RMS, according to the standard IEC 61000-4-7, Appendix C.4). This common RMS is obtained as the square root of the sum of squares of the modules of the components \bar{x} and \bar{y} that add up in this spectral bar, $\sqrt{x^2 + y^2}$; in this example, $\sqrt{13.2^2 + 4.05^2} = 13.808$ V. As can be seen in Figure 2, the values of the amplitude of the resulting vector in each window were generally different from the correct common RMS value and were unstable.

2.2. Analysis of Varying the Position of the Interharmonic Tone

The amplitude variations that appear in the analysis of successive windows (and as a consequence of the spectral leakage produced by a single fixed interharmonic tone) were discussed in the previous section. Next, a similar analysis was made, but varying the frequency of the interharmonic tone of the previous example. The RMS value measured in the spectral bar corresponding to 250 Hz is represented in Figure 3, with a fixed harmonic tone of 13.2 V at the same frequency and a second interharmonic tone of 9.8 V with variable frequency. The values obtained with the DFT on four non-overlapping and consecutive windows 0.2 s long (tw1–tw4) are shown in that figure. These values were obtained using rectangular windows. When the harmonic and variable tones coincide at the origin of abscissa, 250 Hz, the RMS value of their vectorial sum is obtained. For the other variable tone positions that are synchronous with the *tw* window (or multiples of the basic frequency: 255, 260, 265 ... Hz) the harmonic does not receive leakage, and therefore, its value remains stable at 13.2 V. The value obtained is different due to the generated leakage for the rest of the non-synchronous (or interharmonic) positions, with more significant variations the closer is the variable frequency interharmonic tone to the measured spectral bar, located at 250 Hz. Thus, the interaction between tones is more significant when both are closer together (Figure 3, 250–255 Hz spectral bar interval), and smaller variations occur when both tones are far apart (Figure 3, 260–265 Hz, 265–270 Hz). Therefore, in the analysis of a single window, the values obtained in all cases were different from the desired common RMS values, except in variable tone synchronous positions, where there was no leakage (see Figure 3a).

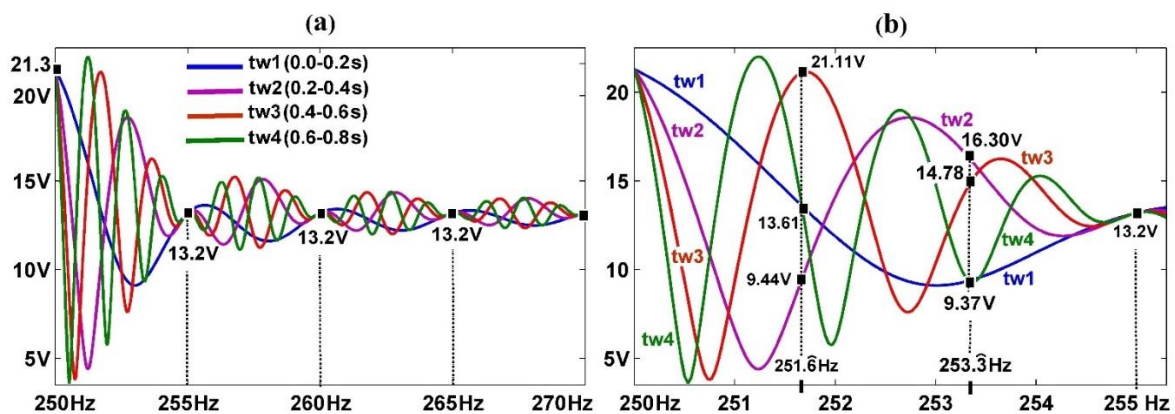


Figure 3. RMS value measured at the 250 Hz spectral bar, with a 13.2 V harmonic fixed in the same position, as a function of the 9.8 V variable frequency tone position, in several successive windows treated individually (tw1–tw4): (a) variable frequency tone positions between 250 and 270 Hz, and (b) zoomed zone between 250 and 255 Hz.

Figure 3b shows a zoom of the area between the harmonic at 250 Hz and the following spectral bar at 255 Hz. It can be seen that the values obtained are the same as in the example in the preceding section when the position of interharmonic sweeping tone was 253.3 Hz: 9.37 V in the window tw1,

16.30 V in tw2, 14.78 V in tw3, 9.37 V again in the window tw4, etc. Figure 3b also highlights the position of the variable tone at 251.6 Hz. In this case, the ideal period T_w is also 0.6 s, and therefore, the RMS values found repeat every three windows. Additionally, the total spectral leakage produced was the same for the positions of the variable tone at 251.6 Hz and 253.3 Hz. However, when the tone was at 251.6 Hz, the variations in the values found in each window were higher, due to its closer proximity to the 250 Hz spectral bar, where the amplitude was actually measured.

In conclusion, in the analysis of a single window, the values obtained change depending on the position of the variable tone and are different from the ones desired, except in the synchronous positions of the tone, in which there is no leakage. Moreover, for the same position of the variable tone, the values obtained are different if they are compared along successive windows, except for the positions in which the tone does not emit leakage (and in general, the positions with distances between tones are multiples of the spectral resolution), as shown in Figure 3.

3. Measurement Improvement by Time Aggregation

3.1. Calculation of the Ideal Aggregation Time to Find the Common RMS Value

In the examples of the previous section, the interactions between tones (interharmonic or not synchronized with the acquisition window) were studied. These interactions are due to the spectral leakage produced by the lack of synchronism, giving rise to variations in the amplitudes of the DFT calculated in each window, and can be large in the case of proximity between tones. This can happen when signals, such as the output of electronic converters, are measured using IEC standards. Therefore, it is necessary to correct and stabilize these amplitude variations to make them as close as possible to the desired and correct common RMS value.

The effects of time aggregation on the processing of frequency groupings were studied next, to demonstrate how to overcome that problem. First, it was proven that the aggregation of the RMS values found in successive windows, for two proximate tones, permits obtaining the correct RMS value of the components of these tones that interact in the same spectral bar.

Let \bar{x} be the harmonic component and \bar{y} the leakage received by \bar{x} . The RMS value of the resulting vector would ideally be equal to $\sqrt{x^2 + y^2}$, as if the angle between the two vectors was 90° . However, the actual phase angle between the two tones is unknown, and the procedure is to divide the time into m short windows and to average the squares of the vectors of each window, making, therefore, a time aggregation of these values, as can be seen in Equation (1).

The relative positions of the vectors are \bar{x}_i and \bar{y}_i , with a phase angle φ_i , which varies as the successive m short time windows.

$$\sqrt{\frac{\sum_{i=0}^{m-1} (\bar{x}_i + \bar{y}_i)^2}{m}} = \sqrt{\frac{m \cdot (x^2 + y^2) + 2 \cdot x \cdot y \cdot \sum_{i=0}^{m-1} \cos(\varphi_i)}{m}} = \sqrt{(x^2 + y^2) + \frac{2 \cdot x \cdot y \cdot \sum_{i=0}^{m-1} \cos(\varphi_i)}{m}} \quad (1)$$

The second term in Equation (1), which depends on the successive positions of the vectors (φ_i), explains the fluctuations of the values, and therefore, it should be as low as possible. This can be achieved in two ways:

- The term $\sum_{i=1}^m \cos(\varphi_i)$ decreases if the total aggregation time coincides with the ideal period T_w (or a multiple), divided into $m = T_w/tw = p$ short windows. In that case, an integer number n of complete phase turns of the leakage (related to the other tone) is obtained. As a result, φ_i increases an average of $(n \cdot 360/p)$ degrees in each evaluated window, so that the resulting angle is given by Equation (2):

$$\varphi_i = \beta + i \cdot (n \cdot 360/p), \quad (2)$$

where $n \cdot 360$ is the total angle rotated by the leakage vector until it is again, in the same relative position with the other harmonic vector and β is the initial phase angle. Then:

$$\sum_{i=0}^{m-1} \cos(\varphi_i) = \sum_{i=0}^{p-1} \cos(\beta + i \cdot n \cdot 360 / p) = 0. \tag{3}$$

This way, for analysis periods equal to or multiples of the ideal T_w , divided into short windows tw , on which the DFT is performed, the common RMS values can be obtained for all the spectral components contained in that T_w period.

- Increasing the number of evaluated windows, m . As vectors are added, in a quantity not multiple of p windows, the RMS value obtained differs from the common or correct, but to a lesser extent as the number of aggregated windows, m , becomes greater.

Since the actual components are unknown in real cases, the number m of aggregated windows is increased to reduce the second term in Equation (1). Next, the cases described in the previous section will be analyzed again, but now applying this solution.

3.2. The Analysis of Time Aggregation to Mitigate the Effects on Amplitude

In the example proposed in Section 2.1, the appropriate number of short windows is three ($p = 0.6 \text{ s} / 0.2 \text{ s} = 3$ windows). The only interharmonic at 253.3 Hz produces the spectral leakage. Its representative vector will rotate, relative to the position of the vector of the other component, at an average rate of $(253.3 - 250) \text{ Hz} \times 0.2 \text{ s} / tw \times 360 / \text{cycle} = 240$ per short window tw . As it can be observed in Figure 2, the initial position of the leakage vector is repeated every three windows; that is, in $3 tw \times 240 / tw = 720$ (two complete turns). The speed of rotation between any two tones is just the difference of frequencies between them, which, multiplied by the ideal period T_w , gives the number of complete turns of one tone with respect to the other until the same relative position between them is reached ($3.3 \text{ Hz} \times 0.6 \text{ s} / T_w = 2$, in the example).

For this example, Table 1 shows the values obtained with each acquisition window, together with the corresponding aggregated values calculated with the modules accumulated up to each window considered, for the spectral bars corresponding to the 5th and 6th harmonics, interharmonic group 5, and the total energy (or sum of all the spectral bars, according to Parseval's theorem).

Table 1. Modules obtained for each acquisition window for the total signal of Figure 1, for different frequency groupings, with and without time aggregation.

Window Number	5th Harmonic (250 Hz)		6th Harmonic (300 Hz)		gIH 5 (255-295 Hz)		Total Vrms	
	Aggregation		Aggregation		Aggregation		Aggregation	
	No	Yes	No	Yes	No	Yes	No	Yes
tw1	9.372	9.372	10.303	10.303	8.574	8.574	16.550	16.550
tw2	16.303	13.297	9.780	10.045	8.537	8.555	21.000	18.906
tw3	14.777	13.808	9.922	10.004	8.497	8.536	19.898	19.243
tw4	9.372	12.843	10.303	10.080	8.574	8.545	16.550	18.606
tw5	16.303	13.606	9.780	10.021	8.537	8.544	21.000	19.109
tw6	14.777	13.808	9.922	10.004	8.497	8.536	19.898	19.243
tw7	9.372	13.265	10.303	10.048	8.574	8.541	16.550	18.882

It can be observed how every three windows, all the values of the modules of each window repeat, and the value aggregated after this third window is repeated after three other windows and so on.

The aggregated values are separated again from the ideal, common RMS value if more windows are added, but while decreasing the error, without it being necessary to stop exactly in one of the windows' multiples of T_w to obtain a good result. The final aggregated value is still an average that approximates the desired common RMS value in all groupings, including that of the total RMS. The approximation is better, the longer the time of the aggregation. In practice, in the signals obtained from real tests, there is a limitation of this time due to the thermal constants of this type of test.

Reaching the true common RMS value does not mean that an interharmonic group such as gIH5 encompasses all the energy released by the interharmonic leakage of 253.3 Hz (9.8 V), as this is only possible if a frequency grouping of the entire spectrum is considered. It means that this common RMS value is correctly measured, as the square root of the sum of squares of the modules of the components that are added in each bar are (for 5th harmonic: $\sqrt{13.2^2 + 4.05^2} = 13.808$ V, as seen in Section 2.1).

Table 1 also indicates the total common RMS value of 19.243 V_{rms}, obtained by adding all the spectral bars and aggregating their values along three windows (which coincides exactly with the theoretical value, $\sqrt{13.2^2 + 9.8^2 + 10^2}$, if all the components of the studied example are considered).

It can be observed that the repetition period to obtain the total common RMS value, containing all the spectral bars, is the same as for each group of frequencies, since only an interharmonic has been considered (that is the cause of the leakage that affects the whole spectrum, and therefore, rotates at the same speed in all the spectral bars). If there were multiple interharmonics, there would be areas of the spectrum with different ideal aggregation time related to other areas and the full spectrum, depending on the proximity and influence of the different interharmonics causing the spectral leakage producing this lack of synchronization.

3.3. An Analysis of Varying the Position of the Interharmonic Tone

Figure 4 shows the RMS value measured at the 250 Hz spectral bar, in which a harmonic tone of 13.2 V_{rms} is kept fixed. This value depends on the frequency of a second variable tone of 9.8 V_{rms}. The individual values found after performing the DFT on each of the first four windows of 0.2 s (tw_1 – tw_4) are shown in that figure, along with those computed after performing the time aggregation on the first three windows (aggregated over time (Aggreg.) tw_1 – tw_3), and those using a higher number of windows (Aggreg. tw_1 – tw_{144}).

Figure 4b shows an enlarged area with the values obtained for the sweeping tone at 253.3 Hz. The time aggregation of three windows (black dotted line) provides the correct common RMS value (13.81 V) for that position, which is also obtained if another quantity multiple of three windows is aggregated (144 in this graph, black continuous line). However, the aggregation of three windows is not sufficient for other positions of the tone closest to the harmonic with which it interacts, as it takes longer aggregation time when both tones are closer.

The most significant variations between values obtained in successive windows occur when the sweeping tone is close to the center of the space between spectral bars, as in those positions, the leakage produced is the highest. Additionally, in those positions, the sum of the vector components of both tones experiences abrupt changes because the rotation speed between the representative vectors of the tones is maximum, so the variations of the phase angles between them are very significant. As the sweep tone approaches the other tone, changes in values between windows become slower, as the phase angle variation is smaller. For small rotation angles (due to the interaction between nearby tones), the evolution of the cosine summation in (1) is slower, and that leads to a more extensive aggregation of windows to improve the calculation of the RMS value. Therefore, $\cos(\varphi_i)$ evolves more slowly for close tones or with low rotation speeds between them, as is observed in Figure 4b when the sweep tone is close to the fixed harmonic located at 250 Hz. In that case, there are smaller variations between the amplitudes obtained with the successive tw_1 – tw_4 windows and a more significant difference between the aggregated value computed with only three windows and the correct RMS value (continuous black line, for a high number of aggregated windows).

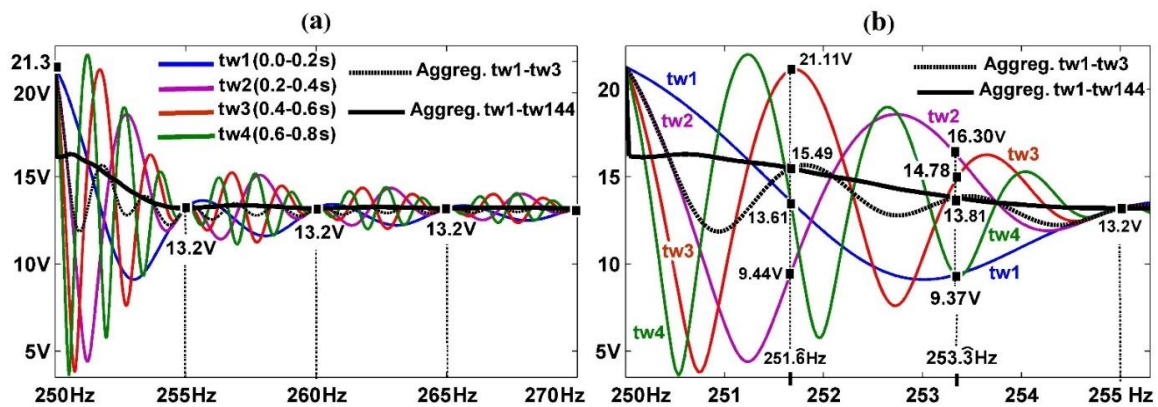


Figure 4. RMS value measured at the 250 Hz spectral bar, with a 13.2 V harmonic fixed in the same position, as a function of the position of the variable frequency tone of 9.8 V, in several successive windows treated individually (tw1–tw4) and aggregated over time (Aggreg.): (a) variable frequency tone positions between 250 and 270 Hz, and (b) zoomed zone between 250 and 255 Hz.

4. Time Aggregation Using the Hann Window

The variability of the amplitude values, obtained with the DFT used in successive analysis windows, when there were several nearby tones whose leakage rotated at different speeds—was not exclusive of the RW. Figure 5 shows the results of applying HW, considering a unitary harmonic tone centered on 50 Hz that interacts with another sweep tone or variable frequency and amplitude unit.

HW has a main lobe that is twice as wide as the RW window, with gain -0.5 in the side spectral bands located at ± 5 Hz of the frequency where the tone is. For this reason, with this window, it is necessary to take into account the group gain [16], with value $\sqrt{1.5}$, in those groupings that add several consecutive spectral bars.

Figure 5 shows a comparison of the RW and HW, where only a sampling window of 0.2 s has been considered (5 Hz resolution), and with a 0° offset between the two tones. A similar oscillation of values can be observed using both windows when the sweep tone is close to the harmonic tone, which is when the two tones interact most. However, with HW, this oscillation extends with more amplitude towards the zones of the lateral spectral bars (between 40 and 60 Hz) due to the more significant interaction of the sidebands of this window. When the sweep tone is at 40 Hz, its upper HW sideband at 45 Hz is added to the lower HW sideband of the harmonic, as it is at 45 Hz; the same can be said at the 55 Hz position when the sweep tone is at 60 Hz. Similarly, when the sweep tone is at 45 Hz, its upper HW sideband at 50 Hz is added to the harmonic, at that same position; and when the sweep tone is at 55 Hz, its lower HW sideband at 50 Hz is also added to the harmonic. Out of these zones, more stable values are obtained with both windows, although with more significant fluctuation in the case of RW. Therefore, the time aggregation is less necessary when the tones are distant and their interaction is lower, even being unnecessary if HW is used.

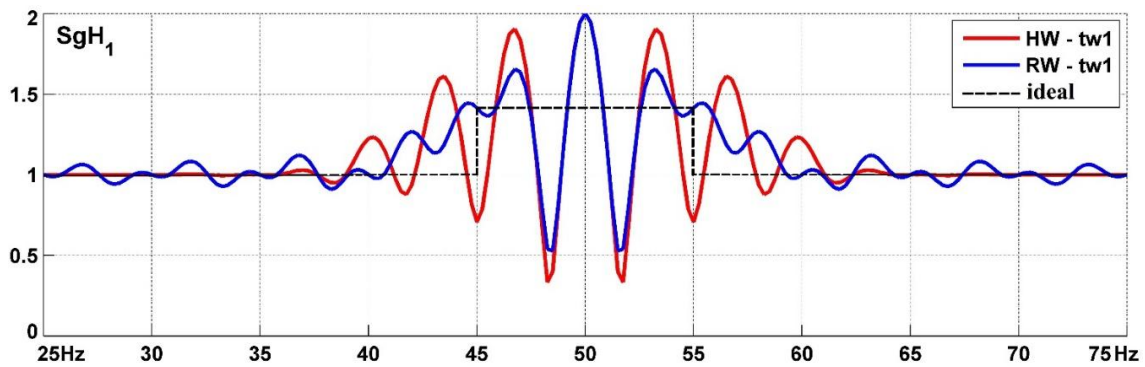


Figure 5. Harmonic subgroup centered in 50 Hz, with the unit harmonic in that position, depending on the position of another unitary tone, for a single 0.2 s window—rectangular window (RW), Hann window (HW), and ideal (black dashed line).

Figure 6a shows a result without aggregation and using a single window. However, if the time aggregation is adequate, results such as those shown in Figure 6b,c,d can be obtained, which are closer to the ideal value (marked with black dashed line in Figure 5). This ideal value should be 1 V_{rms} if no spectral leakage is present for the sweep tone outside the subgroup (between 0 and 45 Hz or higher than 55 Hz), in which only the harmonic remains within the harmonic subgroup measured. The value should be $\sqrt{2}$ when both harmonic and variable components within the subgroup coincide, between 45 and 55 Hz. However, the common RMS value, obtained with time aggregation, is lower than $\sqrt{2}$ when the sweep tone is within the limits of the subgroup and emits spectral leakage outward, and greater than 1 V_{rms} when it is at interharmonic positions outside the subgroup, because part of the leakage gets into the measured subgroup.

Figure 6 illustrates how the results improve with the rectangular window and time aggregation in the transition areas between the subgroup and outside its limits. Yet, HW provides better results inside the subgroup and areas far from it, because it is less sensitive to distant leakage, unlike RW, whose leakage is more widespread.

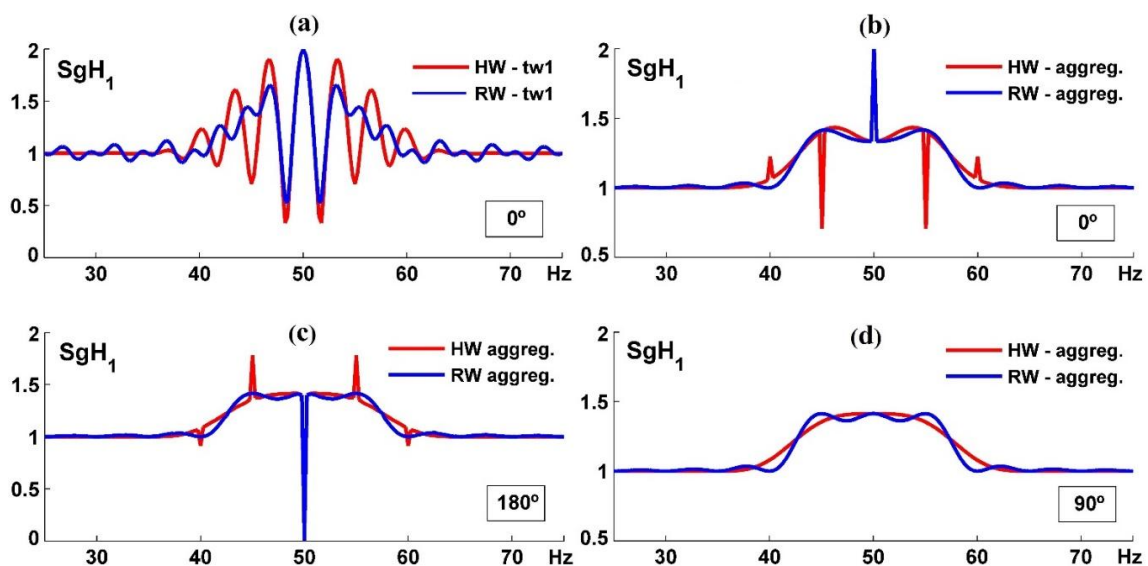


Figure 6. Amplitude calculated using rectangular (RW) and Hann (HW) windows 0.2 s long of a harmonic subgroup centered in 50 Hz, with the unitary harmonic in that position, as a function of the position of another single tone: (a) without aggregation; (b) with time aggregation for the phase angles between tones of 0°, (c) 180°, and (d) 90°.

The phasors of the simulated tones are added when they coincide in the same position (50 Hz in the simulations). The result depends on the phase angle between them. The sum result is maximum if both tones are in phase (Figure 6b) or minimum if the phase angle between them is 180° (Figure 6c). For the rest of phase angles, the summed results are between the former. In the particular case of 90° (Figure 6d), these maxima and minima are not appreciated because the square sum of two tones at 90° is equal to the sum of their squares. To obtain the correct common RMS value, they behave the same way in the position in which both tones at 90° coincide, as in the rest of the positions in which they do not.

In other cases, the values obtained where the position of tone components coincide depend on the particular phase angle between them. With HW, this happens in the position in which their frequencies are equal (50 Hz), and also in the cases in which the lateral bands of the two tones, harmonic and sweeping, coincide, as can be seen in Figure 6b,c.

As a consequence, singular values (or local peaks, according to [16]) appear at the positions of the central harmonic tone, and ± 5 Hz and ± 10 Hz around its position. The interference between the main lobes of the Hann windows of each of the simulated tones explains that result. The variations of these values are maximum when the phase difference between the two tones is 0° or 180° .

In the next section, it is shown how these local peaks generally occur when several spectral components that are distant multiples of the frequency resolution Df interact with each other, and how this happens not only with HW but also with other types of windows, such as RW.

5. Measurement Improvements by Window Overlapping

5.1. Appearance of Local Peaks

In previous sections, the interactions between two frequency components—such as a harmonic (that does not emit leakage) and an interharmonic whose leakage was vectorially added in the position of the harmonic, generating a variable amplitude in the total vector—were analyzed. However, this situation also extends to other frequency components, which interact when added together in the same spectral bar. Examples of these frequency components that interact on the spectral bars of a frequency group are leakage generated by interharmonic tones present within a group being measured; leakage received from other tones located outside the group; or even, if HW is used, sidebands (located within the measured group) of all types of tones, both harmonic and interharmonic, internal and external to the group.

Thus, when several frequency components interact in the same spectral bar, they are vectorially added in that position, generating a total vector whose amplitude depends on their phase angles and frequencies. If these components occupy synchronous positions (therefore, they do not emit spectral leakage), the vector amplitude remains stable. If, on the other hand, the phase angles change and differ at the beginning of each acquisition window, the vector amplitude will also change, and time aggregation will be necessary to find the result closest to the desired common RMS value. This is the case for several tones whose frequency difference (or relative rotation speed) is not a multiple of the frequency resolution, as may occur between a harmonic and an interharmonic, or between several interharmonics (and even harmonics, when there are synchronism errors).

However, if the frequency differences between the spectral components that interact in the same spectral bar are multiples of the frequency resolution, Df , the relative phase between these components do not change between successive windows, and therefore, its total sum vector does not change either. Therefore, time aggregation does not solve these cases, but this may result in inadequate or singular values at the positions of these components, creating local peaks. These peaks may come closer or move away from the correct amplitude value, depending on the phase angle between the tones that cause them. However, most of the time the local peaks move away from the correct common RMS value obtained for other sweep tones, close to each singularity (except for the case of a 90° phase angle between all leakage vectors, in which case the correct RMS value is always obtained).

Figure 7a,b shows an example of these local peaks at distances multiples of 5 Hz between the variable tone and the interharmonic located at 752.5 Hz. Figure 7a illustrates the result using RW, and Figure 7b using HW. Note how the largest local peaks are due to the sidebands of both tones and obtained when HW is used. However, HW generates more local peaks of much smaller amplitude, also at distances multiples of Df . These other peaks are not observed in the figure because this window significantly attenuates the leakage of more distant tones.

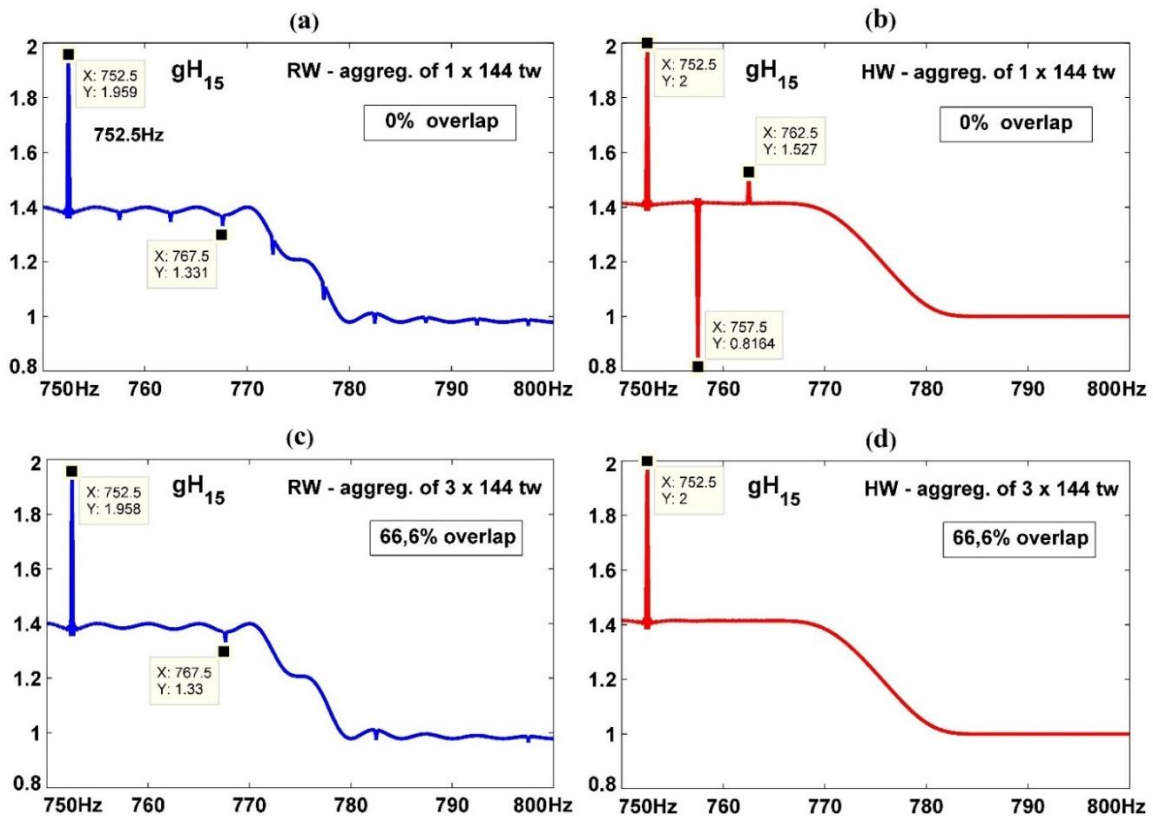


Figure 7. RMS value of harmonic group (gH15, with a fundamental frequency of 50 Hz) as a function of frequency of a sweep tone, with an interharmonic fixed at 752.5 Hz and phase angle 0° , with the rectangular (RW) and Hann (HW) windows and time aggregation: (a,b) without overlap, and (c,d) with 66.66% overlap.

5.2. Local Peak Resolution by Time Aggregation with Window Overlap

An appropriate combination of time aggregation with overlapping between the successive windows analyzed can solve the problems observed in the previous cases. That way, a correct result is achieved for any position of the tones contained in the signal. An overlap of at least 66% and the use of HW eliminates the main, local peaks. Most of them are also removed when using RW.

To explain the following, it must be noted that, for a fixed interharmonic tone f_1 , local peaks in the amplitude may appear due to tones at frequencies $f_1 \pm k \cdot Df$ (with $k = 1, 2, 3 \dots$). Local peaks appear in curves representing RMS values of spectral bars in which the leakage, or sidebands when using HW, of tones separated by $\pm k \cdot Df$ are added.

The representative vector of each tone separated by $\pm k \cdot Df$ rotates $\pm k \cdot 360^\circ$ faster than the central tone f_1 , in each short window tw analyzed. This is because the frequency Df has the window tw as its period, and in a period, the representative vector of a frequency component rotates 360° . Consequently, the relative phase (φ_i in Equation (1)) between the spectral components associated with these tones (\bar{x}_i and \bar{y}_i) does not change at the beginning of the successive windows. The amplitude of their total

sum vector also remains unchanged, independently of the number m of aggregated windows. These points can be seen in Equation (4), with $\varphi_i = \beta \pm i \cdot (k \cdot 360)$ and β the initial phase angle.

$$\sqrt{\frac{\sum_{i=0}^{m-1} (\bar{x}_i + \bar{y}_i)^2}{m}} = \sqrt{x^2 + y^2 + \frac{2 \cdot x \cdot y \cdot \sum_{i=0}^{m-1} \cos(\beta \pm i \cdot k \cdot 360)}{m}} = \sqrt{x^2 + y^2 + 2xy \cos(\beta)}. \quad (4)$$

To solve these cases with time aggregation, it is necessary to change the relative positions (φ_i) between the vectors (\bar{x}_i and \bar{y}_i) of the components that are added in a spectral bar, as seen in Section 3. One solution for resolving local peaks (when tones are at distances multiples of Df) is to use window overlapping to divide each sampling window to cause position changes between the components being added. At that point, the correct common RMS value can finally be obtained with time aggregation, as in the case of tones separated by distances not multiples of Df .

Therefore, if the next window is overlapped with the previous one, dividing the windows into q parts, then the rotation angle in each window will then be $k \cdot 360/q$ for each tone separated by $\pm k \cdot Df$. Then, if q windows are aggregated ($m = q$), the value obtained may coincide with the correct common RMS value, if the sum of cosines in Equation (1) is canceled. For this purpose, the term $k \cdot 360/q$ cannot be multiple of 360° , because then the sum of cosines would never be annulled; that is, the quotient k/q cannot be an integer. Then, for an overlap of tw/q parts of the sampling window (or of $100 \cdot (q-1)/q$ %), the local peaks separated by $\pm k \cdot Df$ Hz can be annulled, for all values of k different from q or a multiple of q .

For example, with $q = 3$ (66.6 % overlap) the singularities at $\pm k \cdot 5$ Hz with k non-multiples of three are solved. That is, all the main local peaks using HW are removed, most of them with RW, leaving singularities at ± 15 Hz (and their multiples) of the fixed tone (see Figure 7c,d). With $q = 4$, (75% overlap) the singularities at ± 5 , ± 10 and ± 15 Hz and their multiples are solved, except the multiples at ± 20 Hz (see Figure 8c).

Therefore, to resolve the existing local peaks up to a distance of $\pm (q-1) \cdot Df$ Hz between the two tones (and multiples of these distances, except those of $\pm q \cdot Df$), an overlap of $(q-1) \cdot 100/q$ % is required. Table 2 summarizes the local peaks resolved for the first levels of window overlapping.

Table 2. Distances between tones, separated by k multiples of the frequency resolution Df , in which local peaks are produced and resolved for different window overlaps: resolved cases (·) and unresolved ones (X).

	k																							
q	1	2	3	4	5	6	7	8	9	10	11	12	13	14	15	16	17	18	19	20	21	22	23	24
2	·	X	·	X	·	X	·	X	·	X	·	X	·	X	·	X	·	X	·	·	·	X	·	X
3	·	·	X	·	·	X	·	·	X	·	·	X	·	·	X	·	·	X	·	·	X	·	·	X
4	·	·	·	X	·	·	·	X	·	·	·	X	·	·	·	X	·	·	·	X	·	·	·	X
5	·	·	·	·	X	·	·	·	·	X	·	·	·	·	X	·	·	·	·	X	·	·	·	·
6	·	·	·	·	·	X	·	·	·	·	·	X	·	·	·	·	·	X	·	·	·	·	·	X
7	·	·	·	·	·	·	X	·	·	·	·	·	·	X	·	·	·	·	·	·	·	X	·	·
8	·	·	·	·	·	·	·	X	·	·	·	·	·	·	·	X	·	·	·	·	·	·	·	X

Figure 8 shows how, for any number of fixed interharmonic tones (located at 708 Hz, 734 Hz, and 747 Hz in this example) and with different angle phases related to the sweep tone (of 0° , 45° , and 180° , respectively), the overlap allows one to resolve, simultaneously, the local peaks, independently of their positions and phases. When HW is used (in red), a 75% overlap is enough to eliminate all the main local peaks simultaneously. In the case of RW (in blue) and a 75% overlap, only local peaks remain when the sweep tone is located at ± 20 Hz (and their multiples) of each preset tone.

Window overlapping does not modify the benefits of time aggregation for the rest of spectral components (distanced not multiples of the resolution) since when aggregating with overlapping,

what is done is to average the squares of the values obtained in several sequences of consecutive windows, displaced according to the percentage of overlapping. For example, for a 75% overlap, the values obtained in four sequences of consecutive windows, shifted $tw/4$ between them, are aggregated and averaged by the total number of windows used (in this case, four times the number of windows used in a single sequence). Thus, in order not to cancel out the beneficial effects of time aggregation applied to the rest of tones, it would be ideal to keep the previous number $p = Tw/tw$ of windows (aggregating without overlapping) and repeat it q times in order to also eliminate local peaks when using the overlapping of tw/q parts of windows.

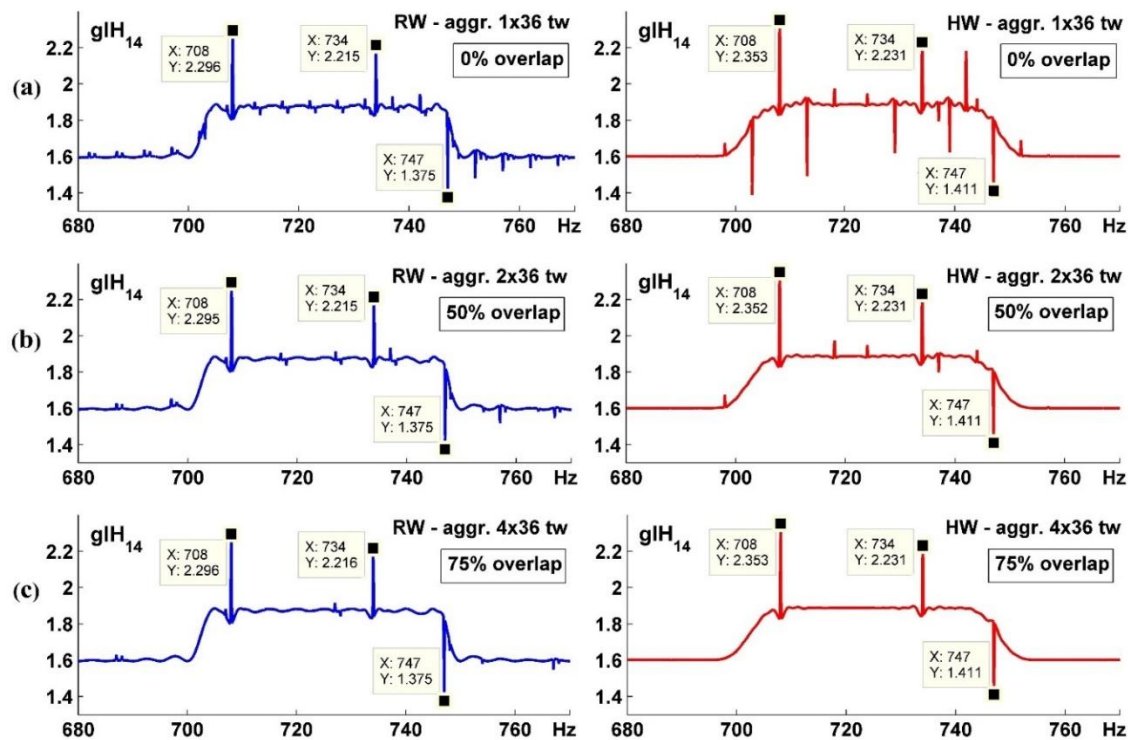


Figure 8. RMS value of an interharmonic group as a function of sweep tone, with several interharmonics with different delays and positions, with time aggregation using the rectangular window (blue) and the Hann window (red): (a) no overlapping, (b) with overlapping at 50%, and (c) with overlapping at 75%.

In real cases, if the number of windows aggregated is sufficiently high (although not the ideal one), the values obtained will approach the correct RMS value for all the frequencies, including the local peaks that are annulled by the overlap used in each case. The only uncanceled local peaks are those of the spectral bars wherein components of several tones that have precisely the same frequency are added together, since it is not possible to distinguish them from the case in which they are a single tone.

To understand the importance of overlapping to resolve local peaks, it is necessary to consider the rich interharmonic content at the output of inverters feeding induction motors; domestic equipment, such as low-consumption lamps; or even converters that are connected to the grid, in the case of solar panels or wind power plants. Using the IEC standard, two nearby spectral bars are separated multiples of $Df = 5$ Hz (that is, relatively large frequencies); therefore, for each interharmonic tone in a nearby area of the spectrum, there are multiple positions, separated by $\pm k Df$ from that tone, in which erroneous values would be obtained. Even if an adequate time aggregation is used, it would not solve the issue of obtaining the appropriate common RMS value for such groupings in which these local peaks coincide, unless the aggregation and overlap are combined adequately between the windows aggregated in time.

6. Case Study

As a complement to the previous examples, in which synthetic signals based on examples appearing in the IEC Standard were used, an experimental study has been carried out. An induction motor was tested by being fed from two inverters with different harmonic contents—Allen Bradley's PowerFlex 40 (sinusoidal PWM modulation type) and Telemecanique's Altivar 66 (random carrier frequency modulation); thus, obtaining a greater variety of harmonic contents. The motor used was a Siemens 0.75 kW, star connected, with rated values of 50 Hz, 400 V, and 1.86 A. A magnetic powder brake was used as a load, adjusted so that part of the tests were carried out with low load (motor slip close to 0.3%), and others with high load (slip around 4%). The acquisition system was based on a National Instruments PCI6250 card, plus an external interface module with LEM Hall Effect sensors used as transducers. The acquired data was processed using Matlab R2015 software.

The induction motor used mixed eccentricity, which produces great interharmonic content in the low part of the current spectrum, which, together with the abundant harmonic and interharmonic content in the high part of the spectrum present in the output of the inverters, allowed us analyzing situations with a multitude of nearby tones and similar amplitudes. The motor operated at steady state during 60 s long tests, and the sampling frequency was 80 kS/s.

All measurements were made at the output of the inverters, with fundamental frequencies and harmonic contents different from those of the mains signal, so it was necessary to adapt the analysis system, based on IEC standards, and orient it to the measurement of the utility network; to the specific characteristics of the signals. Figure 9 shows the laboratory test bench.

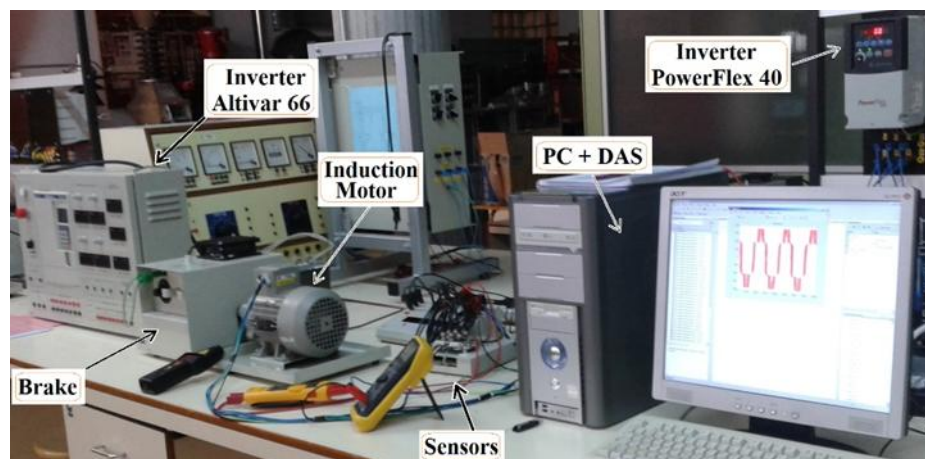


Figure 9. Laboratory test bench.

Figure 10a shows the low part of the frequency response of the output current of the induction motor fed by a PowerFlex inverter with slip $s \approx 4\%$ and a fundamental frequency of 45 Hz. Figure 10b shows the low part of the frequency response of the output voltage of the Altivar inverter working at 55 Hz and with low loaded motor ($s \approx 0.3\%$). The frequency responses were obtained based on the IEC standard, (using DFT, with spectral bars separated by 5 Hz), not yet grouped by frequency. It can be seen that the interharmonic content was much higher for the current signal (Figure 10a) than for the voltage signal (Figure 10b). Therefore, high values of the groupings and current rates containing those frequencies were to be expected, and a greater interaction between tones, which motivates an increase in the aggregation time necessary to obtain stable values, as explained before. On the other hand, the tone interaction was predicted to be lower in the case of Figure 10b, since the voltage measured in that zone presents practically only harmonics (which do not interact with each other, as they do not produce spectral leakage).

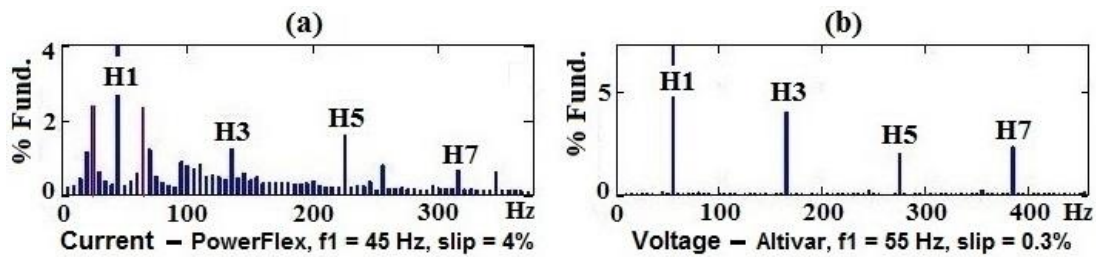


Figure 10. Low part of the frequency response of the supply signals from two inverters connected to an induction motor: (a) current with PowerFlex, (b) voltage with inverter Altivar.

Figure 11 presents the time evolution, using 0.2 s long windows, of the harmonic distortion rates for low frequencies (THD (Total Harmonic Distortion) of current (Figure 11a) and voltage (Figure 11b)), measured at the output of the inverters of the same tests of Figure 10. RW was used in the graphs on the left and HW in the graphs on the right. Blue indicates the values without time aggregation or corresponding to each analysis window. In red, the values aggregated until each instant are shown so that it is possible to observe the value of any size of aggregation up to 60 s (duration of the test). The aggregated values for 3 s and 60 s, as well as the window number corresponding to each aggregation time, are highlighted in all graphs.

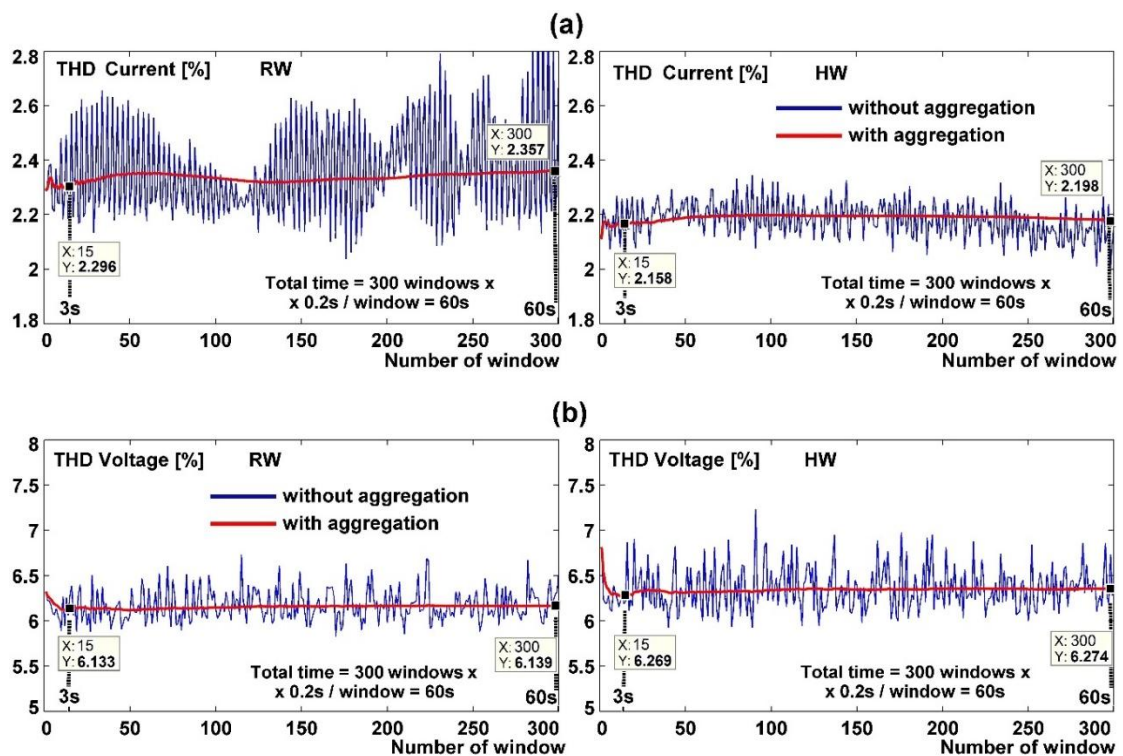


Figure 11. Time evolution of: (a) the THD current rate of the PowerFlex inverter, and (b) the THD voltage rate of the Altivar inverter, for the same tests shown in Figure 10.

In tests whose spectra present harmonics surrounded by abundant interharmonics, of relatively large amplitudes and comparable to those of harmonics and close to them (as, for example, occurs in the test corresponding to Figure 10a), large differences were observed between the values found in each individual window for rates such as THD (blue graphs in Figure 11a). This is because the leakage produced by these interharmonics is also large, and when absorbed by nearby harmonics, vectorially adding to them, gives rise to variable amplitudes, and therefore, more aggregation time would be needed, as indicated in the previous sections. Thus, it was observed how the aggregated values obtained in the Figure 11a test were stabilized for a time greater than 3 s, which would justify

the use of longer aggregation times. On the other hand, the rate measured in Figure 11b reached a stable value more quickly, due to the lower interharmonic content of the analyzed signal (Figure 10b), in which case the aggregation time of 3 s was sufficient.

These tests prove experimentally that the aggregation time required for some parameters measured at the output of inverters may be greater than the 3 s indicated in the standard, and considerably less than the 10 min indicated in the same IEC standard for the next recommended time grouping.

7. Discussion

The correct measurement of the network harmonic content is important to characterizing the energy supplied, for example, at the output of frequency converters, as this type of equipment is the source of high harmonic and interharmonic content that makes analysis very challenging.

The existing regulations establish procedures for adequate measurement, describing both the spectral groupings and the necessary time groupings, but problems may arise that make the measurements obtained unreliable. One of them is the instability and inaccuracy of the amplitude values obtained with DFTs in successive sampling windows, due to spectral leakage, and which affect the groupings and distortion rates based on IEC standards. A second problem is the possible occurrence of local peaks due to interharmonic tones that are distanced from each other by multiples of the spectral resolution, and therefore, are not affected by time aggregation, as a way of obtaining reliable RMS values.

The evolution of the values of the groupings defined by the IEC standards has been studied to describe these problems and propose solutions. The study focused on the relative position between interharmonics and harmonics, and their relationship with the time of aggregation and type of window.

Time aggregation is not necessary when a single frequency component is contained in the frequency grouping measured, since in that case, there is no interference between different components, and therefore, the RMS value obtained is stable and reliable. Examples of these frequency components are a tone present within the measured grouping, the spectral leakage received from another tone outside the grouping, or, if HW is used, a sideband to a tone. However, with more than one component within any of the groupings defined in the standards (such as several interharmonics whose leakages rotate at different speeds) each spectral bar will receive those leakages. Therefore, the total vector obtained in that bar will be the sum of the contributions of all the leakages, causing the variation of its amplitude in each successive analysis window.

Therefore, it is convenient to perform time aggregation in all spectral groupings to minimize the effects of leakage on the resulting amplitudes, and to obtain a reliable and stable RMS value. Such time aggregation should be applied to all groups and subgroups, harmonics and interharmonics, and all distortion rates, as these rates are composed of those normalized groupings. That way, DFT amplitude variation caused by spectral leakage decreases, and the final aggregated value is closer to the correct RMS one.

However, the ideal aggregation period T_w is unknown in practical applications or differs depending on the area of the spectrum, type of signal (either from the network or from the output of a converter), and the rest of the conditions of each test. Besides, the 61000-4-30 standard proposes aggregation time values as distant as 3 s to 2 h, so the specific duration of this aggregation time for each particular case is open to modification. Time aggregation must be adapted to the thermal time constants of the connected equipment. When thermal time constants are short, as in industrial environments, it is preferable to use the 3 s aggregation interval; the 10 min aggregation interval is best used to evaluate systems with longer time constants, such as the public electric network.

For this reason, even based on quality standards, the necessary modifications must be made to adapt the values recommended in these standards to the particular case of measurements on systems consisting of frequency converters supplying induction motors. For all the above reasons, a solution has been proposed to the problems of instability and imprecision in the RMS values, obtained with the DFT according to IEC standards: the use of time aggregation with an increase in the aggregation time

with respect to the 3 s recommended by the regulations for signals in industrial environments. This proposal improves the results for all cases with interacting tones.

On the other hand, the sensitivity analysis of several tones interacting shows differences between RW and HW similar to those studied with a single tone, provided that an appropriate time aggregation is carried out beforehand. HW provides values closer to the ideals in interior areas and further away from the frequency groupings, whereas RW provides better results in the transition between groupings.

In specific cases where the interacting tones are separated by multiples of the frequency resolution, local peaks are produced, which most often deviate from the correct value obtained for other sweep tones close to each singularity. This second problem can be solved by an appropriate combination of time aggregation with overlapping between successive analyzed windows. This approach provides an enhanced response for all harmonic and interharmonic positions of the tones present in the signal. Overlapping of 75% is an advisable value, for its being one of the most used, as indicated in [46], and for allowing the elimination of the most notable local peaks of RW and all the important ones of HW.

Consequently, with the proposal presented in this work, which consists of carrying out an adequate time aggregation with overlapping, it is possible to obtain a response closer to the ideal in all the frequency groupings defined in the regulations, and thus obtain more reliable and precise measures in their related distortion rates. This is especially necessary for signals such as the output of electronic converters, which are rich in nearby tones, whose leakage can interact, causing this problem, especially those using some types of modulations, such as closed-loop or random modulations, or when connected to faulty motors that cause additional harmonic content.

It has been experimentally proven that the aggregation time required for some parameters measured at the output of the tested drives may be greater than the 3 s indicated in the standard, and considerably less than the 10 min indicated in the same IEC standard for the next recommended time grouping. The duration of the tests carried out was 1 min because the thermal constants of the equipment tested resulted in aggregation times shorter than this time. It has also been verified that, in areas of the spectrum with stable harmonics and low interharmonic content, the aggregation time may be shorter.

Author Contributions: Conceptualization, A.A.-G., O.D.-P., D.M.-S., and A.Z.-L.; data curation, A.A.-G.; methodology, A.A.-G., O.D.-P., and D.M.-S.; software, A.A.-G.; validation, D.M.-S.; writing—original draft, A.A.-G.; writing—reviewing and editing, O.D.-P., D.M.-S., and A.Z.-L.

Funding: This research was partially funded by Universidad de Valladolid.

Conflicts of Interest: The authors declare no conflict of interest.

References

1. Blaabjerg, F.; Yang, Y.; Yang, D.; Wang, X. Distributed Power-Generation Systems and Protection. *Proc. IEEE* **2017**, *105*, 1311–1331. [[CrossRef](#)]
2. Rönnerberg, S.; Bollen, M. Power quality issues in the electric power system of the future. *Electr. J.* **2016**, *29*, 49–61. [[CrossRef](#)]
3. Otcenasova, A.; Bolf, A.; Altus, J.; Regula, M. The Influence of Power Quality Indices on Active Power Losses in a Local Distribution Grid. *Energies* **2019**, *12*, 1389. [[CrossRef](#)]
4. Kalair, A.; Abas, N.; Kalair, A.R.; Saleem, Z.; Khan, N. Review of harmonic analysis, modeling and mitigation techniques. *Renew. Sustain. Energy Rev.* **2017**, *78*, 1152–1187. [[CrossRef](#)]
5. Rönnerberg, S.K.; Bollen, M.H.J.; Amaris, H.; Chang, G.W.; Gu, I.Y.H.; Kocewiak, Ł.H.; Meyer, J.; Olofsson, M.; Ribeiro, P.F.; Desmet, J. On waveform distortion in the frequency range of 2 kHz–150 kHz—Review and research challenges. *Electr. Power Syst. Res.* **2017**, *150*, 1–10. [[CrossRef](#)]
6. Collin, A.J.; Djokic, S.Z.; Drapela, J.; Langella, R.; Testa, A. Proposal of a Desynchronized Processing Technique for Assessing High Frequency Distortion in Power Systems. *IEEE Trans. Instrum. Meas.* **2019**, *68*, 3883–3891. [[CrossRef](#)]
7. Guo, Q.; Wu, J.; Jin, H.; Peng, C. An innovative calibration scheme for interharmonic analyzers in power systems under asynchronous sampling. *Energies* **2019**, *12*, 121. [[CrossRef](#)]

8. Ravindran, V.; Busatto, T.; Ronnberg, S.K.; Meyer, J.; Bollen, M. Time-varying interharmonics in different types of grid-tied PV inverter systems. *IEEE Trans. Power Deliv.* **2019**. [[CrossRef](#)]
9. Jain, S.K.; Singh, S.N. Harmonics estimation in emerging power system: Key issues and challenges. *Electr. Power Syst. Res.* **2011**, *81*, 1754–1766. [[CrossRef](#)]
10. Chen, C.I.; Chen, Y.C. Comparative study of harmonic and interharmonic estimation methods for stationary and time-varying signals. *IEEE Trans. Ind. Electron.* **2014**, *61*, 397–404. [[CrossRef](#)]
11. Liu, Y.; Wang, X.; Liu, Y.; Cui, S. Resolution-enhanced harmonic and interharmonic measurement for power quality analysis in cyber-physical energy system. *Sensors* **2016**, *16*, 946. [[CrossRef](#)]
12. Stanisavljević, A.M.; Katić, V.A.; Dumnić, B.P.; Popadić, B.P. Overview of voltage dips detection analysis methods. In Proceedings of the 2017 International Symposium on Power Electronics (Ee), Novi Sad, Serbia, 19–21 October 2017.
13. International Electrotechnical Commission (IEC). *IEC Standard 61000-4-7: General Guide on Harmonics and Interharmonics Measurements, for Power Supply Systems and Equipment Connected Thereto*; IEC: Geneva, Switzerland, 2002.
14. International Electrotechnical Commission (IEC). *IEC Standard 61000-4-30: Testing and Measurement Techniques—Power Quality Measurement Methods*; IEC: Geneva, Switzerland, 2015.
15. Tarasiuk, T. A few remarks about assessment methods of electric power quality on ships—Present state and further development. *Measurement* **2009**, *42*, 1153–1163. [[CrossRef](#)]
16. Testa, A.; Gallo, D.; Langella, R. On the Processing of Harmonics and Interharmonics: Using Hanning Window in Standard Framework. *IEEE Trans. Power Deliv.* **2004**, *19*, 28–34. [[CrossRef](#)]
17. Gallo, D.; Langella, R.; Testa, A. On the processing of harmonics and interharmonics in electrical power systems. In Proceedings of the 2000 IEEE Power Engineering Society Winter Meeting, Singapore, 23–27 January 2000.
18. Gallo, D.; Langella, R.; Testa, A. Double stage harmonic and interharmonic processing technique. In Proceedings of the 2000 Power Engineering Society Summer Meeting, Seattle, WA, USA, 16–20 July 2000.
19. Barros, J.; Diego, R.I. On the use of the Hanning window for harmonic analysis in the standard framework. *IEEE Trans. Power Deliv.* **2006**, *21*, 538–539. [[CrossRef](#)]
20. Barros, J.; Diego, R.I. Effects of windowing on the measurement of harmonics and interharmonics in the IEC standard framework. In Proceedings of the 2006 IEEE Instrumentation and Measurement Technology Conference, Sorrento, Italy, 24–27 April 2006.
21. Bracale, A.; Carpinelli, G.; Leonowicz, Z.; Lobos, T.; Rezmer, J. Measurement of IEC Groups and Subgroups Using Advanced Spectrum Estimation Methods. *IEEE Trans. Instrum. Meas.* **2008**, *57*, 672–681. [[CrossRef](#)]
22. Tarasiuk, T. Comparative study of various methods of DFT calculation in the wake of IEC standard 61000-4-7. *IEEE Trans. Instrum. Meas.* **2009**, *58*, 3666–3677. [[CrossRef](#)]
23. Moreira Monteiro, H.L.; Manso Silva, L.R.; Duque, C.A.; De Andrade Filho, L.M.; Fernando Ribeiro, P. Comparison of interpolation methods in time and frequency domain for the estimation of harmonics and interharmonics according to IEC standard. In Proceedings of the 2014 16th International Conference on Harmonics and Quality of Power (ICHQP), Bucharest, Romania, 25–28 May 2014.
24. Chicco, G.; Russo, A.; Spertino, F. Supraharmonics: Concepts and experimental results on photovoltaic systems. In Proceedings of the 2015 International School on Nonsinusoidal Currents and Compensation (ISNCC), Lagow, Poland, 15–18 June 2015.
25. Alfieri, L.; Bracale, A.; Carpinelli, G.; Larsson, A. Accurate assessment of waveform distortions up to 150 kHz due to fluorescent lamps. In Proceedings of the 2017 6th International Conference on Clean Electrical Power (ICCEP), Santa Margherita Ligure, Italy, 27–29 June 2017.
26. Klatt, M.; Meyer, J.; Schegner, P. Comparison of measurement methods for the frequency range of 2 kHz to 150 kHz. In Proceedings of the 2014 16th International Conference on Harmonics and Quality of Power (ICHQP), Bucharest, Romania, 25–28 May 2014.
27. Shadmehr, H.; Chiameo, R.; Belloni, F.R. Beyond FFT algorithm in analyzing harmonics at frequency range of 2 kHz to 500 kHz. In Proceedings of the 2018 18th International Conference on Harmonics and Quality of Power (ICHQP), Ljubljana, Slovenia, 13–16 May 2018.
28. Chicco, G.; Schlabbach, J.; Spertino, F. Experimental assessment of the waveform distortion in grid-connected photovoltaic installations. *Sol. Energy* **2009**, *83*, 1026–1039. [[CrossRef](#)]

29. Spertino, F.; Chicco, G.; Ciocia, A.; Malgaroli, G.; Mazza, A.; Russo, A. Harmonic distortion and unbalance analysis in multi-inverter photovoltaic systems. In Proceedings of the 2018 International Symposium on Power Electronics, Electrical Drives, Automation and Motion (SPEEDAM), Amalfi, Italy, 20–22 June 2018.
30. Soltani, H.; Davari, P.; Zare, F.; Blaabjerg, F. Effects of Modulation Techniques on the Input Current Interharmonics of Adjustable Speed Drives. *IEEE Trans. Ind. Electron.* **2018**, *65*, 167–178. [[CrossRef](#)]
31. Oliveira, W.R.; Filho, A.L.F.; Cormane, J. A contribution for the measuring process of harmonics and interharmonics in electrical power systems with photovoltaic sources. *Int. J. Electr. Power Energy Syst.* **2019**, *104*, 481–488. [[CrossRef](#)]
32. Bartman, J.; Kwiatkowski, B. The Influence of Measurement Methodology on the Accuracy of Electrical Waveform Distortion Analysis. *Meas. Sci. Rev.* **2018**, *18*, 72–78. [[CrossRef](#)]
33. Dalali, M.; Jalilian, A. Indices for measurement of harmonic distortion in power systems according to IEC 61000-4-7 standard. *IET Gener. Transm. Distrib.* **2015**, *9*, 1903–1912. [[CrossRef](#)]
34. Langella, R.; Testa, A.; Meyer, J.; Moller, F.; Stiegler, R.; Djokic, S.Z. Experimental-Based Evaluation of PV Inverter Harmonic and Interharmonic Distortion Due to Different Operating Conditions. *IEEE Trans. Instrum. Meas.* **2016**, *65*, 2221–2233. [[CrossRef](#)]
35. Soltani, H.; Blaabjerg, F.; Zare, F.; Loh, P.C. Effects of Passive Components on the Input Current Interharmonics of Adjustable-Speed Drives. *IEEE J. Emerg. Sel. Top. Power Electron.* **2016**, *4*, 152–161. [[CrossRef](#)]
36. Chicco, G.; Pons, E.; Russo, A.; Spertino, F.; Porumb, R.; Postolache, P.; Toader, C. Assessment of unbalance and distortion components in three-phase systems with harmonics and interharmonics. *Electr. Power Syst. Res.* **2017**, *147*, 201–212. [[CrossRef](#)]
37. Grevener, A.; Meyer, J.; Rönnberg, S. Comparison of Measurement Methods for the Frequency Range 2–150 kHz (Supraharmonics). In Proceedings of the 2018 IEEE 9th International Workshop on Applied Measurements for Power Systems (AMPS), Bologna, Italy, 26–28 September 2018.
38. Holmes, G.; Lipo, T. *Pulse Width Modulation for Power Converters: Principles and Practice*; Wiley-IEEE Press: Piscataway, NJ, USA, 2003; ISBN 0471208140.
39. Leon, J.I.; Kouro, S.; Franquelo, L.G.; Rodriguez, J.; Wu, B. The Essential Role and the Continuous Evolution of Modulation Techniques for Voltage-Source Inverters in the Past, Present, and Future Power Electronics. *IEEE Trans. Ind. Electron.* **2016**, *63*, 2688–2701. [[CrossRef](#)]
40. John, M.; Mertens, A. Frequency-Domain Model of Voltage-Source Inverters with Closed-Loop Current Control. In Proceedings of the 2018 IEEE 19th Workshop on Control and Modeling for Power Electronics (COMPEL), Padua, Italy, 25–28 June 2018.
41. Lee, K.; Shen, G.; Yao, W.; Lu, Z. Performance Characterization of Random Pulse Width Modulation Algorithms in Industrial and Commercial Adjustable-Speed Drives. *IEEE Trans. Ind. Appl.* **2017**, *53*, 1078–1087. [[CrossRef](#)]
42. Huang, Y.; Xu, Y.; Zhang, W.; Zou, J. Hybrid RPWM Technique Based on Modified SVPWM to Reduce the PWM Acoustic Noise. *IEEE Trans. Power Electron.* **2019**, *34*, 5667–5674. [[CrossRef](#)]
43. Liu, Y.; Bazzi, A.M. A review and comparison of fault detection and diagnosis methods for squirrel-cage induction motors: State of the art. *ISA Trans.* **2017**, *70*, 400–409. [[CrossRef](#)]
44. Liu, J.; Leng, Y.; Lai, Z.; Fan, S. Multi-frequency signal detection based on Frequency Exchange and Re-Scaling Stochastic Resonance and its application to weak fault diagnosis. *Sensors* **2018**, *18*, 1325. [[CrossRef](#)]
45. Merizalde, Y.; Hernández-Callejo, L.; Duque-Perez, O. State of the art and trends in the monitoring, detection and diagnosis of failures in electric induction motors. *Energies* **2017**, *10*, 1056. [[CrossRef](#)]
46. Harris, F.J. On the use of windows for harmonic analysis with the discrete Fourier transform. *Proc. IEEE* **1978**, *66*, 51–83. [[CrossRef](#)]

